# Observational Evidence for a Correlation between the Magnetic Field of Jets and Star Formation Rate in Host Galaxies

Yongyun Chen (陈永云)[1] , Qiusheng Gu (顾秋生)[2], Junhui Fan (樊军辉)[3], Xiaotong Guo (郭晓通)[4], Xiaoling Yu (俞效龄)[1], Nan Ding (丁楠)[5], and Dingrong Xiong (熊定荣)[6]

[1] College of Physics and Electronic Engineering, Qujing Normal University, Qujing 655011, People's Republic of China; ynkmcyy@yeah,net
[2] School of Astronomy and Space Science, Nanjing University, Nanjing 210093, People's Republic of China; qsgu@nju.edu.cn
[3] Center for Astrophysics, Guangzhou University, Guangzhou 510006, People's Republic of China
[4] Anqing Normal University, Anhui 246133, People's Republic of China
[5] School of Physical Science and Technology, Kunming University, Kunming 650214, People's Republic of China
[6] Yunnan Observatories, Chinese Academy of Sciences, Kunming 650011, People's Republic of China

Abstract

Accretion supermassive black holes in the center of active galaxies usually produce "jet"-collimated bipolar outflows of relativistic particles. Magnetic fields near the black hole event horizon may play a crucial role in the formation of jets/outflows. Both theory and observation indicate that jets/outflows driven by centrally active supermassive black holes have a feedback effect on the overall properties of the host galaxies. Therefore, the magnetic field is a key ingredient for the formation and evolution of galaxies. Here, we report a clear correlation between the magnetic field of jets and star formation rate for a large sample of 96 galaxies hosting supermassive black holes, which suggests that the star formation of active galactic nuclei host galaxies may be powered by the jets.

Unified Astronomy Thesaurus concepts: Active galactic nuclei (16); Star formation (1569); Supermassive black holes (1663); AGN host galaxies (2017)

1. Introduction

In the past few decades, the importance of magnetic fields in star formation has been a controversial topic. In two papers, Mestel (1965a, 1965b) argued for the importance of magnetic fields in star formation (L. Mestel 1965a, 1965b). He pointed out that the average region of the interstellar medium (ISM) containing a stellar amount of mass cannot simply collapse to stellar density because it contains too much angular momentum. He believes that the magnetic field may play a vital role in eliminating angular momentum from interstellar material to allow star formation. C. F. McKee & E. C. Ostriker (2007) suggested that magnetic fields have a major effect in extracting the angular momentum of the accreting gas and cause a large amount of accretion gas to form stars.

The magnetic field is closely related to star formation. Some authors have found that the magnetic field enhances star formation (S. Niklas & R. Beck 1997; D. J. Bomans & M. Krause 2007; K. T. Chyży 2008; K. T. Chyży et al. 2011; D. R. G. Schleicher & R. Beck 2013; V. Heesen et al. 2014; F. S. Tabatabaei et al. 2017; V. Heesen & T. L. Klocke 2023). D. R. G. Schleicher & R. Beck (2013) proposed a theoretical explanation for the observational relationship between magnetic field strength (B) and star formation rate (SFR) surface density (Σ_{SFR}). This B–SFR relation is $B \propto \Sigma_{SFR}^{1/3}$. They assumed that the kinetic energy density of a gas is regulated by star formation, so this relationship is the result of saturation of small-scale dynamo. However, as pointed out by U. P. Steinwandel et al. (2020), a similar relationship is found when the magnetic field is amplified only by adiabatic compression. Due to the rapid

amplification of the magnetic field through turbulence, the small-scale dynamo is thought to have provided a strong magnetic field during the formation of the first stars and galaxies (R. Beck et al. 1996; T. G. Arshakian et al. 2009; D. R. G. Schleicher et al. 2010; J. Schober et al. 2012; M. A. Latif et al. 2013). However, F. S. Tabatabaei et al. (2018) found that there is an anticorrelation between the equipartition magnetic field and SFR for NGC 1097. They suggested the massive star formation quenching by nonthermal effects in the center of NGC 1097. At present, there has been ongoing debate on whether magnetic fields have an impact on star formation. There has always been a lack of large samples to study the relationship between magnetic fields and the SFR of active galactic nuclei (AGN) host galaxies.

Observations have found that jets/outflows have both negative (M. Cano-Diaz et al. 2012; S. Carniani et al. 2016; M. Bischetti et al. 2022; Z. Chen et al. 2022; C. Lammers et al. 2023) and positive (S. Croft et al. 2006; I. J. Feain et al. 2007; Rodriguez Zaurin et al. 2007; D. Elbaz et al. 2009; M. Imanishi et al. 2011; R. M. Crockett et al. 2012; P. C. Zinn et al. 2013; Z. Schutte & A. E. Reines 2022; G. Venturi et al. 2023) feedback effects on the host galaxies of AGN. The theoretical model of relativistic jets in AGN suggests that the jets/outflows mainly come from the spin of the black hole, the mass of the central black hole, and the magnetic field near the event horizon of the black hole (R. D. Blandford & R. L. Znajek 1977). X. Cao (2018) suggested that the jets can be accelerated by the magnetic field. Moreover, the magnetic field plays an important role in regulating the star formation process on galactic scales. The magnetic fields regulate the transport of highly energetic particles and are essential in any theory of star formation (M. R. Krumholz & C. Federrath 2019). At the same time, the magnetic field strength established by small-scale dynamo may contribute greatly to the observed correlation between SFR and magnetic field strength in galaxies

(D. R. G. Schleicher & R. Beck 2013). M. Livio et al. (1999) suggested that the large-scale field of the jet can be produced from the small-scale field created by dynamo processes. Therefore, there may be a correlation between the magnetic field of the jet and star formation. In this paper, we use a large sample of 96 galaxies hosting supermassive black holes to study the relation between the magnetic field of the jets and SFR. The second part describes the samples; the third part describes the results and discussions; and the fourth part is the conclusion. Throughout the paper, we adopt a cosmology with $H_0 = 70 \, \mathrm{km \, s^{-1} \, Mpc^{-1}}$, $\Omega_m = 0.3$, and $\Omega_\Lambda = 0.7$.

2. The Sample

The jets associated with these supermassive black holes have well-determined magnetic fields of the jets and the host galaxies have reliable redshifts. These galaxies hosting supermassive black holes come from the catalog of A. B. Pushkarev et al. (2012) and M. Zamaninasab et al. (2014). At the same time, we consider that these sources have multiband photometric data. We obtain the SFR and stellar mass of the host galaxies of a supermassive black hole by fitting multiband spectral energy distribution (SED) data. Table 1 lists the properties of 96 galaxies hosting supermassive black holes, including stellar mass and SFRs of host galaxies.

2.1. Calculating the Magnetic Field from the Core-shift Measure

According to the standard model of relativistic jets (R. D. Blandford 1979), the observation position of the radio core is a function of the observation frequency. This frequency-dependent core position shift can be used to estimate magnetic field strength and electron number density (A. P. Lobanov 1998; K. Hirotani 2005). This method is based on several simple and reasonable assumptions: the flow is conical, the half opening angle θ_j is small, and Γ remains constant (without significant acceleration or deceleration). In addition, it is assumed that the magnetic field strength and electron number density decrease with the increase of the distance from the central engine and follow the power function relationship: $B(z) = B_{1 \, \mathrm{pc}}(z/1 \, \mathrm{pc})^{-\alpha_b}$, $n_e(z) = n_{1 \, \mathrm{pc}}(z/1 \, \mathrm{pc})^{-\alpha_n}$, where z is the distance from the black hole (M. Zamaninasab et al. 2014). Here, $B_{1 \, \mathrm{pc}}$ and $n_{1 \, \mathrm{pc}}$ represent the magnetic field strength and electron number density of the jet frame at a distance of 1 pc away from the apex of the jet. These assumptions lead to the power-law behavior of the core shift as a function of the observation frequency (A. P. Lobanov 1998), $r_{\mathrm{core}} \propto \nu^{-1/k_r}$, where r_{core} is the absolute position of the radio core and k_r is the core-shift index. The so-called "core-shift" effect can be performed via high-angular-resolution radio observations (A. P. Lobanov 1998), i.e., it shifts upstream at higher frequencies and downstream at lower frequencies (A. B. Pushkarev et al. 2012). The observed shift (in milliarcseconds) of the core between ν_1 and ν_2 ($\Delta r_{\mathrm{core}, \nu_1 \nu_2}$) is defined using $|\mathrm{CS}| = \Delta r_{\mathrm{core}, \nu_1 \nu_2}$, where $|\mathrm{CS}|$ is the absolute core shift. The CS is $\mathrm{CS} = \mathrm{IS} - \mathrm{OS}$ (A. B. Pushkarev et al. 2012), where IS is the image shift and OS is the difference in the coordinates (offset shift relative to the map center). If the apparent core positions measured at two frequencies ν_1, ν_2 ($\nu_1 < \nu_2$) differ by $\Delta r_{\mathrm{core}, \nu_1 \nu_2}$, the core position shift ($\Omega_{r\nu}$) is estimated using the

following formula,

$$\Omega_{r\nu} = 4.85 \times 10^{-9} \left[\frac{\Delta r_{\mathrm{core}, \nu_1 \nu_2} D_L}{(1 + z_*)^2} \right] \left[\frac{\nu_1^{1/k_r} \nu_2^{1/k_r}}{\nu_2^{1/k_r} - \nu_1^{1/k_r}} \right] \mathrm{pc \, GHz}, \tag{1}$$

where D_L is the luminosity distance, and z_* is the redshift of sources (note we use z_* for redshift to distinguish it from the cylindrical coordinate z).

If the magnetic field decays at a distance of z^{-1} as expected by the azimuthal dominant magnetic field, and the energy ratio of magnetic particles to nonthermal particles remains constant, then it is expected that $k_r = 1$. Many observations have indeed revealed the $k_r = 1$ behavior of core movement, supporting the hypothesis that there exists an azimuthal dominant magnetic field in the radio core region (Y. Y. Kovalev et al. 2008; S. P. O'Sullivan & D. C. Gabuzda 2009; K. V. Sokolovsky et al. 2011). Assuming equipartition between magnetic energy and particle energy at the radio core position, based on the above assumption of the scaling of magnetic field and relativistic electron density with distance, the jet frame magnetic field strength at 1 pc from the black hole can be estimated through the following formula (K. Hirotani 2005; S. P. O'Sullivan & D. C. Gabuzda 2009),

$$B_{1 \, \mathrm{pc}} \simeq 0.025 \left(\frac{\Omega_{r\nu}^3 (1 + z)^2}{\theta_j \delta^2 \sin^2 \theta} \right)^{1/4}, \tag{2}$$

where θ is the viewing angle, and δ is the Doppler factor. It is assumed that the jet spectral index $\alpha_{\mathrm{jet}} = -0.5$. The Doppler factor is $\delta = \Gamma^{-1}(1 - \beta \cos\theta)^{-1}$ and the apparent jet speed is $\beta_{\mathrm{app}} = \beta \sin\theta (1 - \beta \cos\theta)^{-1}$ (A. B. Pushkarev et al. 2012). For the estimate of the magnetic field, we assume that the jet is viewed at the critical angle (A. B. Pushkarev et al. 2012) $\theta \simeq \Gamma^{-1}$. This yields (A. B. Pushkarev et al. 2012)

$$B_{1 \, \mathrm{pc}} \simeq 0.042 \Omega_{r\nu}^{3/4} (1 + z)^{1/2} (1 + \beta_{\mathrm{app}}^2)^{1/8}. \tag{3}$$

2.2. The Stellar Mass and SFR of AGN Host Galaxies

We derive the stellar masses and SFRs of the host galaxies using version 2022.0 of the SED-fitting code CIGALE[7] (D. Burgarella et al. 2005; S. Noll et al. 2009; M. Boquien et al. 2019). We use the optical photometry data from Pan-STARRS1–DR1 Surveys (K. C. Chambers et al. 2016). The IR data was taken with the Two Micron All Sky Survey (2MASS; M. F. Skrutskie et al. 2006) and Wide-field Infrared Survey Explorer (WISE; E. L. Wright et al. 2010). Consequently, we have 12 photometric data (g, r, i, z, y_{P1}, J, H, K/Ks, and 3.4, 4.6, 12, and 22 μm) for the SED fitting. In our work, we use the templates of galaxy + AGN to fit the SEDs of our sample. The template for galaxies is composed of four modules, including star formation history, single stellar population model (G. Bruzual & S. Charlot 2003), dust attenuation (D. Calzetti et al. 2000), and dust emission (B. T. Draine & A. Li 2007; D. A. Dale et al. 2014). The module used for the component of AGN is J. Fritz et al. (2006). These modules are all included in CIGALE. We use the parameters and values given in Table 2 to define the CIGALE grid of model galaxy SEDs. CIGALE

---

[7] https://cigale.lam.fr/

Table 1
The Sample of Galaxies Hosting Supermassive Black Holes

Name	R.A.	Decl.	z_*	$B_{1\,pc}$	log SFR$_{sed}$	log M_*	$\beta_{app}(c)$	$\Omega_{r\nu}$ (pc GHz)
(1)	(2)	(3)	(4)	(5)	(6)	(7)	(8)	(9)
QSO B0003-066	1.557886944	−6.393148611	0.347	<0.2	2.495	11.26	2.89	<4.55
QSO B0106+013	17.16154611	1.583423056	2.099	<0.79	3.057	12.58	26.5	<7.86
QSO B0119+115	20.4233125	11.83067	0.57	1.63	3.115	11.24	17.1	37.75
QSO B0133+476	24.244145	47.85808333	0.859	0.77	3.381	11.84	12.98	13.69
QSO B0149+218	28.07524583	22.11880556	1.32	1.69	3.594	11.8	18.55	29.64
QSO B0202+149	31.21005806	15.23640111	0.405	0.48	1.999	10.66	6.41	10.87
QSO B0212+735	34.37838944	73.82572806	2.367	1.27	3.389	12.54	7.64	21.24
QSO B0224+671	37.20854806	67.35084139	0.523	0.75	2.605	11.1	11.63	15.47
QSO B0238-084	40.269994	−8.255764	0.005	0.015	−0.379	9.01	0.23	0.226
QSO B0333+321	54.12544833	32.30815056	1.259	1.95	3.648	12.11	12.76	41.51
QSO B0336-019	54.8789075	−1.776612222	0.852	0.92	3.326	11.51	22.36	14.41
QSO B0403-132	61.39169917	−13.13715694	0.571	1.54	2.871	10.46	19.69	33.3
QSO B0420-014	65.81583639	−1.342518056	0.914	1.41	3.174	12.61	7.36	35.94
QSO B0528+134	82.73506972	13.53198583	2.07	1.6	3.851	12.04	19.2	22.71
QSO B0607-157	92.42062306	−15.71129778	0.324	0.68	2.186	11.16	3.93	21.22
QSO B0716+714	110.4727019	71.34343417	0.31	0.49	3.237	12.68	10.06	10.16
QSO B0736+017	114.8251414	1.617949444	0.191	<0.2	1.427	10.92	14.32	<2.94
QSO B0738+313	115.2945969	31.20006361	0.631	0.81	3.542	10.55	10.76	16.85
QSO B0748+126	117.7168572	12.51800806	0.889	0.84	3.472	11.64	18.37	13.49
QSO B0754+100	119.2776789	9.943014444	0.266	0.88	2.423	10.51	14.4	20.38
QSO B0805-077	122.0647333	−7.852746111	1.837	2.71	4.446	12.02	50.6	34.84
QSO B0804+499	122.1652764	49.84348083	1.436	0.48	1.972	11.45	1.83	11.5
QSO B0823+033	126.4597431	3.156811389	0.506	0.83	3.604	10.77	17.8	15.57
QSO B0827+243	127.7170258	24.18328333	0.94	1.18	2.981	12	22.01	19.64
QSO B0836+710	130.3515219	70.89504806	2.218	1.93	3.349	12.27	25.38	25.72
QSO B0851+202	133.7036456	20.10851139	0.306	<0.28	2.989	11.7	15.17	<4.18
QSO B0859-140	135.5701458	−14.25859472	1.339	1.7	3.922	10.31	16.47	30.96
QSO B0906+015	137.2920483	1.359893889	1.024	1.61	3.522	12.59	20.68	29.45
QSO B0917+624	140.4009625	62.26449444	1.446	1.09	3.245	10.79	15.57	16.99
QSO B0923+392	141.7625581	39.03912556	0.695	<0.33	2.525	12.13	4.29	<6.64
QSO B0945+408	147.2305756	40.66238528	1.249	1.1	3.789	12.01	18.6	17.02
QSO B0953+254	149.2078142	25.25445833	0.712	<0.42	2.854	10.89	11.52	<6.71
QSO B1015+359	154.5457458	35.71096139	1.226	0.92	3.689	10.95	12.46	15.55
IVS B1036+054	159.6949164	5.208079444	0.473	0.74	1.609	11.47	6.15	19.26
QSO B1038+064	160.3215106	6.171367778	1.265	1.19	3.501	9.92	11.87	21.97
QSO B1045-188	162.0275858	−19.15992417	0.595	0.86	3.087	11.11	8.57	19.94
QSO B1101+384	166.1138081	38.20883306	0.031	0.1	1.291	8.95	0.82	2.81
QSO B1127-145	172.5293639	−14.82428444	1.184	0.84	2.984	12.5	14.18	13.24
QSO B1150+812	178.30208	80.974765	1.25	0.68	2.608	11.25	7.09	12.34
QSO B1156+295	179.88264	29.24551	0.73	1.17	3.367	12.81	24.73	20.11
QSO B1219+285	185.38204	28.23292	0.102	0.08	−0.956	11.38	4.05	1.39
QSO B1219+044	185.5939317	4.221062222	0.965	0.81	2.725	10.96	2.35	24.16
QSO B1222+216	186.2268733	21.37957778	0.432	0.9	3.296	11.06	21.1	17.03
QSO B1228+126	187.70593	12.391123	0.004	0.012	−1.662	8.86	0.24	0.132
QSO B1253-055	194.0465275	−5.7893125	0.536	<0.42	2.754	12.93	20.57	<5.88
QSO B1302-102	196.3875625	−10.55539639	0.278	0.7	2.858	10.72	5.41	20.34
QSO B1308+326	197.6194328	32.34549528	0.997	0.96	2.981	11.85	27.17	13.61
QSO B1334-127	204.4157614	−12.95685917	0.539	1.23	3.496	11.52	10.26	31.08
QSO B1413+135	213.9950731	13.33992028	0.247	0.44	2.539	10.45	1.8	15.7
QSO B1458+718	224.7815733	71.67218139	0.904	0.51	2.298	11.53	7.04	9.46
QSO B1502+106	226.1040825	10.49422194	1.839	0.69	3.345	12.08	14.77	8.5
QSO B1504-166	226.7700294	−16.87524111	0.876	0.66	1.865	11.38	4.31	15.9
QSO B1508-055	227.7232975	−5.718726944	1.191	1.52	3.449	11.69	18.64	26.81
QSO B1510-089	228.2105539	−9.099952778	0.36	0.73	2.755	12.8	20.14	13.5
QSO B1532+016	233.7185569	1.517835278	1.42	1.14	3.262	11.98	14.11	18.81
QSO B1538+149	235.2062139	14.79609	0.605	0.49	2.904	11.27	8.73	9.25
QSO B1546+027	237.3726533	2.61699	0.414	<0.32	2.814	11.4	12.08	<5.09
QSO B1606+106	242.1925133	10.48549333	1.226	0.79	2.817	12.46	18.91	10.97
QSO B1633+382	248.8145542	38.13458361	1.814	1.62	3.702	13.24	29.45	21.21
QSO B1637+574	249.5560681	57.33999417	0.751	0.71	3.308	11.97	10.61	13.51
QSO B1642+690	250.5327022	68.94437667	0.751	<0.48	1.785	11.32	16.65	<6.85
QSO B1641+399	250.7450414	39.81027611	0.593	1.2	2.968	11.57	19.27	23.85

Table 1
(Continued)

Name	R.A.	Decl.	z_*	$B_{1\,\mathrm{pc}}$	log SFR$_{\mathrm{sed}}$	log M_*	$\beta_{\mathrm{app}}(c)$	$\Omega_{r\nu}$ (pc GHz)
(1)	(2)	(3)	(4)	(5)	(6)	(7)	(8)	(9)
QSO B1652+398	253.4675694	39.76016917	0.033	0.1	−0.377	10.97	0.21	3.25
QSO B1655+077	254.5375478	7.690983611	0.621	0.47	1.174	10.82	14.45	7.45
QSO B1726+455	261.8652117	45.51103667	0.717	<0.28	0.603	10.86	1.82	<6.73
QSO B1730-130	263.2612739	−13.08043	0.902	1.69	3.166	9.35	35.69	27.31
QSO B1749+701	267.136835	70.09743556	0.77	1.04	3.017	12.32	6.03	27.03
QSO B1749+096	267.8867439	9.6502025	0.322	0.33	2.207	12.27	6.84	6.92
QSO B1803+784	270.19035	78.46778306	0.68	<0.39	2.738	12.18	8.97	<6.58
QSO B1807+698	271.7111694	69.82447472	0.051	0.12	0.656	10.34	0.1	3.81
QSO B1823+568	276.0294503	56.850415	0.664	0.74	2.804	11.02	20.85	11.79
QSO B1828+487	277.3821867	48.74637556	0.692	0.69	2.431	12.31	13.65	12.24
QSO B1845+797	280.53746	79.77142	0.057	0.089	1.2	10.35	2.29	1.65
QSO B1849+670	282.3169681	67.09491111	0.657	0.52	2.422	11.71	30.63	6.48
QSO B1928+738	291.9520633	73.96710278	0.302	0.54	2.837	10.95	8.43	12.31
QSO B2005+403	301.9372708	40.49683639	1.736	2.34	3.815	12.15	12.21	47.18
QSO B2037+511	309.6543114	51.32018417	1.686	<0.45	1.534	12.52	3.3	<7.98
QSO B2113+293	318.8725564	29.5606575	1.514	1.16	4.024	11.6	1.4	37.78
QSO B2121+053	320.9354892	5.589470278	1.941	1.43	3.776	12.71	13.29	22.61
QSO B2128-123	322.8969239	−12.11799889	0.501	0.98	3.35	11.84	6.94	26.41
QSO B2131-021	323.5429564	−1.888121944	1.285	1.02	3.081	11.41	20.02	14.94
QSO B2134+004	324.1607756	0.698394444	1.932	1.31	3.463	12.25	5.94	26.23
QSO B2136+141	324.7554553	14.39333111	2.427	<0.55	2.871	12.41	5.43	<7.68
QSO B2145+067	327.0227444	6.960723333	0.99	<0.34	2.91	12.16	2.52	<7.48
QSO B2155-152	329.5261744	−15.01925778	0.672	1.89	3.386	11.97	18.11	43.23
QSO B2200+420	330.6803808	42.27777222	0.069	0.09	1.785	10.83	10.57	1.21
QSO B2201+315	330.8123986	31.76063194	0.295	0.95	2.51	10.7	7.87	27.04
QSO B2201+171	330.8620569	17.43006889	1.076	1.55	3.775	13.18	2.55	54.08
QSO B2209+236	333.0248597	23.92792889	1.125	0.39	1.357	11.63	3.43	7.69
QSO B2223-052	336.4469136	−4.950386389	1.404	1.47	3.005	13.03	17.34	24.63
QSO B2227-088	337.4170181	−8.548454444	1.56	1.44	3.76	12.6	8.14	29.6
QSO B2230+114	338.15173	11.73076917	1.037	2.12	4.477	12.25	15.41	46.48
QSO B2243-123	341.5759875	−12.11424778	0.632	0.78	2.049	11.17	5.49	20.1
QSO B2251+158	343.4906167	16.14821139	0.859	1.13	3.536	12.17	14.19	22
QSO B2345-167	357.0108689	−16.52000611	0.576	0.9	2.736	10.29	13.45	18.44
QSO B2351+456	358.5903392	45.88450778	1.986	1.72	3.729	11.67	18.01	25.97

Note. Column (1): name; column (2): the R.A. in decimal degrees; column (3): (delineation) in decimal degrees; column (4): redshift; column (5): magnetic field strength 1 pc away from the jet base (in units Gauss); column (6): logarithm of star formation rate is estimated by fitting SED; column (7): logarithm of stellar mass; column (8): apparent velocity of the jet; column (9): core-shift measure.

identifies the best-fit SED model by minimizing the χ^2 statistic. We present the example of the best SED fitting in Figure 1.

3. Results and Discussions

We use linear regression to analyze the relationship between the SFR and jet magnetic field in galaxies hosting supermassive black holes. Figure 2 shows the relation between SFR and jet magnetic field in our sample galaxies. A fit to the relation between the two variables is done using linmix[8] (B. C. Kelly 2007). We assume that there is a significant correlation between the two variables when $p < 0.01$. There is a significant correlation between SFR and the magnetic field of the jet for our sample galaxies (Pearson correlation coefficient $r = 0.87$, $p = 5.01 \times 10^{-30}$),

$$\log \mathrm{B}_{1\,\mathrm{pc}} = 0.33(\pm 0.02)\log \mathrm{SFR}_{\mathrm{sed}} - 1.08(\pm 0.05). \quad (4)$$

The tests of Spearman ($r = 0.82$, $p = 1.64 \times 10^{-24}$) and Kendall tau ($r = 0.62$, $p = 3.19 \times 10^{-19}$) also show a significant

---

[8] https://linmix.readthedocs.io/en/latest/

correlation between SFR and magnetic field of the jets for our sample galaxies. Our results suggest that the star formation may occur along the trajectory of the jet. Theoretical models indicate that relativistic jets rely on the magnetic field of black holes (e.g., R. D. Blandford & R. L. Znajek 1977). Our results may imply that jets induce star formation. P. C. Zinn et al. (2013) found that AGN with pronounced radio jets exhibit a much higher SFR, which implies that positive AGN feedback plays an important role (jet-induced star formation). V. Gaibler et al. (2012) found jet-induced star formation through numerical simulation of feedback from AGN.

The relation between SFR and stellar mass for our sample galaxies is shown in Figure 3. The yellow and green lines show the main sequences of star formation at $z \sim 1$ and $z \sim 0$ (D. Elbaz et al. 2007), respectively. From Figure 3, we find that almost all sources are located above the main sequence of star formation. This indicates that the host galaxies of these sources have high SFRs and may be undergoing star formation. We also estimate the specific SFR (sSFR = SFR/M_*). The relation between the sSFR and magnetic field of the jets for our sample
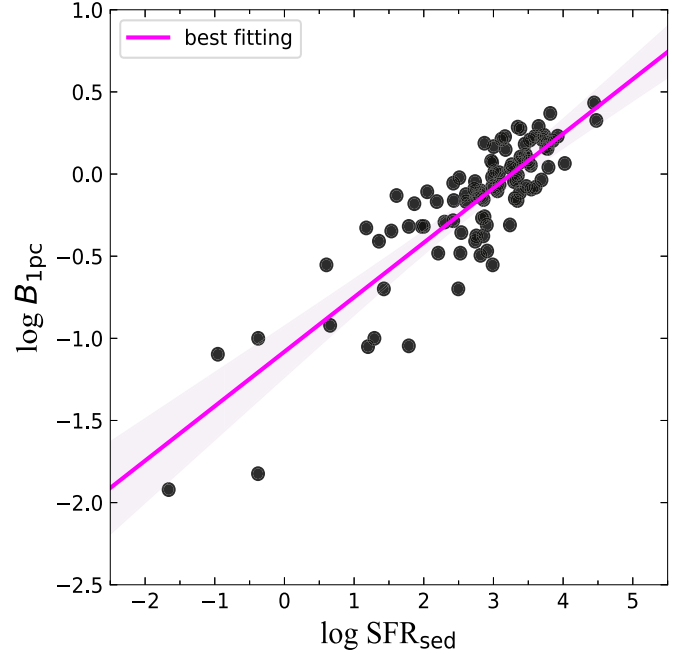
Table 2
CIGALE Grid Parameter Values Adopted for the Modeling Described

Parameter	Values	Description
	Star formation history: Delayed	
τ_{main}	5–8000 (in steps of 10)	e-folding time of the main stellar population model (Myr).
Age	200–13,260 (in steps of 10)	Age of the oldest stars in the galaxy (Myr).
	Single-age stellar population (SSP): G. Bruzual & S. Charlot (2003)	
imf	1	Initial mass function (G. Chabrier 2003)
Metallicity	0.02	Solar
Separation Age	10	Age of the separation (to differentiate) between the young and the old star populations (Myr).
	Dust attenuation: D. Calzetti et al. (2000)	
$E(B-V)_{young}$	0.001, 0.01, 0.015, 0.02, 0.04, 0.06, 0.1, 0.2, 0.3, 0.4, 0.5, 0.6, 0.7, 0.8, 0.9, 1.0	Color excess of the stellar continuum light for the young population.
	Dust emission: D. A. Dale et al. (2014)	
α	2.0, 2.1, 2.5	Alpha from the power-law distribution ($dM_d \propto U^{-\alpha}dU$, with M_d being the dust mass, and U the radiation field intensity).
	AGN model: J. Fritz et al. (2006)	
R_{max}/R_{min}	10.0, 30.0, 60.0, 100.0, 150.0	Ratio of the maximum to minimum radii of the dust torus.
τ	0.1, 0.3, 0.6, 1.0, 2.0, 3.0, 6.0, 10.0	Optical depth at 9.7 μm.
β	−1.00, −0.75, −0.50, −0.25, 0.00	Beta from the power-law density distribution for the radial component of the dust torus (Equation (3) of J. Fritz et al. 2006).
γ	0.0, 2.0, 4.0, 6.0	Gamma from the power-law density distribution for the polar component of the dust torus (Equation (3) of J. Fritz et al. 2006).
Opening Angle (θ)	60.0, 100.0, 140.0	Full opening angle of the dust torus (Figure 1 of J. Fritz et al. 2006).
ψ	0.001, 10.1, 20.1, 30.1, 40.1, 50.1, 60.1, 70.1, 80.1, 89.990	Angle between equatorial axis and line of sight.
f_{AGN}	0.0, 0.05, 0.1, 0.15, 0.2, 0.25, 0.3, 0.35, 0.4, 0.45, 0.5, 0.55, 0.6, 0.65, 0.7, 0.75, 0.8, 0.85, 0.9, 0.95, 0.99	Fraction of AGN torus contribution to the IR luminosity (fracAGN in Equation (1) of L. Ciesla et al. 2015)
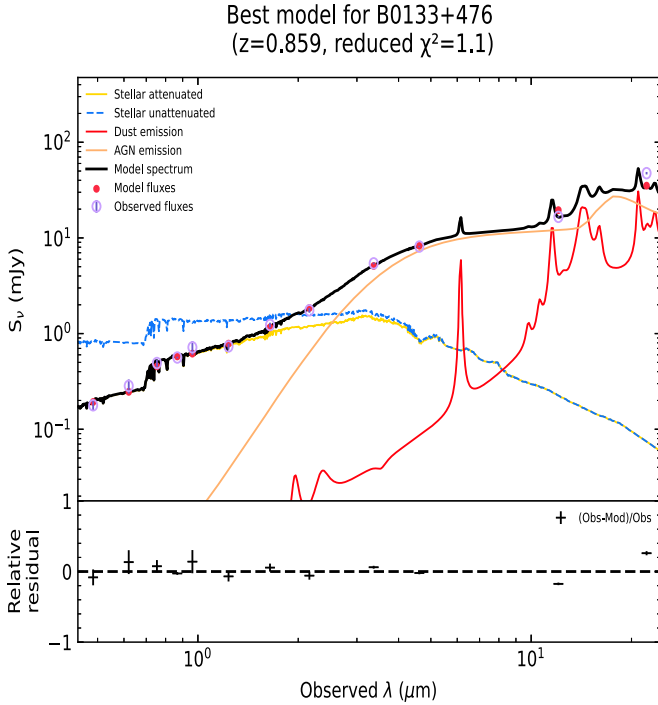
**Figure 1.** The example of broadband SEDs of AGN is modeled by using CIGALE.

Figure 2. Relation between star formation rate and the magnetic field of the jets for galaxies hosting supermassive black holes. The star formation rate is estimated by fitting SED using CIGALE. The $B_{1 pc}$ is the jet's comoving frame magnetic field measured by the core-shift effect. Shaded red colored areas correspond to 3σ confidence bands. The red line is the best fit.

galaxies is shown in Figure 4. We also use linear regression to analyze the relationship between the sSFR and jet magnetic field in galaxies hosting supermassive black holes. There is a significant correlation between sSFR and the magnetic field of the jet for our sample galaxies (Pearson correlation coefficient

$r = 0.47, p = 1.18 \times 10^{-6}$),
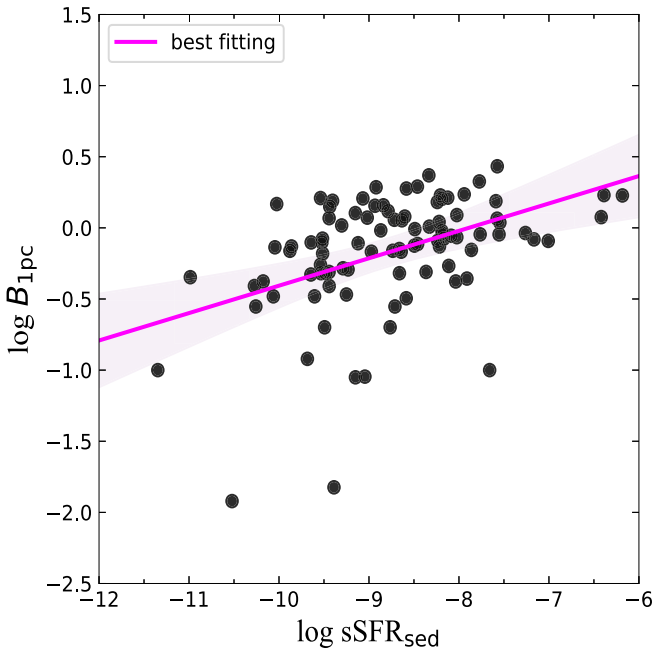
$$\log B_{1 pc} = 0.19(\pm 0.04)\log sSFR_{sed} + 1.52(\pm 0.33). \quad (5)$$

The tests of Spearman ($r = 0.46, p = 1.92 \times 10^{-6}$) and Kendall tau ($r = 0.32, p = 4.63 \times 10^{-6}$) also show a significant
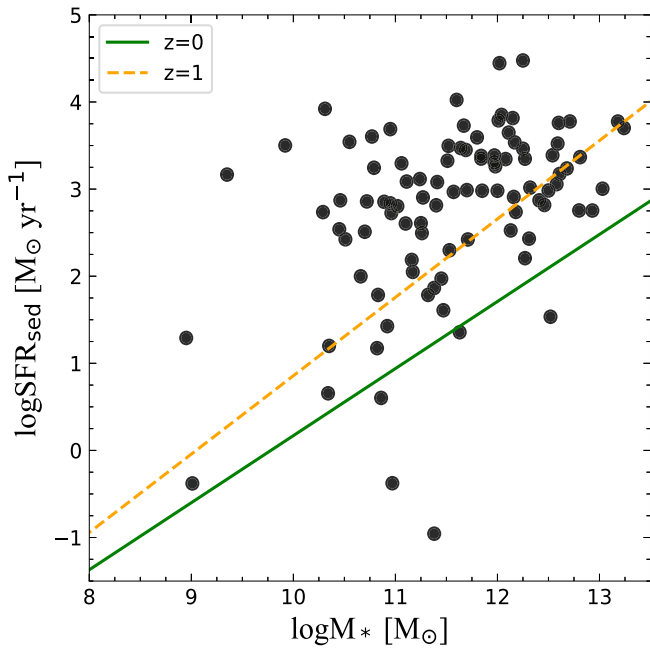
Figure 3. Relation between star formation rate and stellar mass for galaxies hosting supermassive black hole. The yellow and green lines show the main sequences of star formation at $z = 1$ and $z = 0$ (D. Elbaz et al. 2007), respectively.

Figure 4. Relation between specific star formation rate and magnetic field for galaxies hosting supermassive black holes. Shaded red colored areas correspond to 3σ confidence bands. The red line is the best fit.

correlation between sSFR and magnetic field of the jets for our sample galaxies. Our results may provide a new clue for future research about the influence of magnetic fields on star formation using theory and numerical simulations.

4. Conclusions

We fit multiband data to obtain a large sample of star masses and SFRs of galaxies hosting supermassive black holes and

study the relationship between SFRs and the magnetic field of the jets. Our main results are as follows:

(1) We find a significantly strong correlation between the magnetic field of the jets and SFR. The magnetic field strength is proportional to the SFR, $B_{1\,pc} \propto SFR_{sed}^{0.33 \pm 0.02}$. Our results suggest that the jets may induce star formation of AGN host galaxies.

(2) There is also a significantly strong correlation between the magnetic field of the jets and sSFR. The magnetic field strength is proportional to the sSFR, $B_{1\,pc} \propto sSFR_{sed}^{0.19 \pm 0.04}$.

ORCID iDs

Yongyun Chen (陈永云) ⓘ https://orcid.org/0000-0001-5895-0189

References

Arshakian, T. G., Beck, R., Krause, M., & Sokoloff, D. 2009, A&A, 494, 21
Beck, R., Brandenburg, A., Moss, D., Shukurov, A., & Sokoloff, D. 1996, ARA&A, 34, 155
Bischetti, M., Feruglio, C., D'Odorico, V., et al. 2022, Natur, 605, 244
Blandford, R. D. 1979, ApJ, 232, 34
Blandford, R. D., & Znajek, R. L. 1977, MNRAS, 179, 433
Boquien, M., Burgarella, D., Roehlly, Y., et al. 2019, A&A, 622, A103
Bruzual, G., & Charlot, S. 2003, MNRAS, 344, 1000
Burgarella, D., Buat, V., & Iglesias-Páramo, J. 2005, MNRAS, 360, 1413
Calzetti, D., Armus, L., Bohlin, R. C., et al. 2000, ApJ, 533, 682
Cano-Dìaz, M., Maiolino, R., Marconi, A., et al. 2012, A&A, 537, L8
Cao, X. 2018, MNRAS, 473, 4268
Carniani, S., Marconi, A., Maiolino, R., et al. 2016, A&A, 591, A28
Chabrier, G. 2003, PASP, 115, 763
Chambers, K. C., Magnier, E. A., Metcalfe, N., et al. 2016, arXiv:1612.05560
Chen, Z., He, Z., Ho, L. C., et al. 2022, NatAs, 6, 339
Chyży, K. T. 2008, A&A, 482, 755
Chyży, K. T., Bomans, D. J., Krause, M., et al. 2007, A&A, 462, 933
Chyży, K. T., Weżgowiec, M., Beck, R., & Bomans, D. J. 2011, A&A, 529, A94
Ciesla, L., Charmandaris, V., Georgakakis, A., et al. 2015, A&A, 576, A10
Crockett, R. M., Shabala, S. S., Kaviraj, S., et al. 2012, MNRAS, 421, 1603
Croft, S., van Breugel, W., de Vries, W., et al. 2006, ApJ, 647, 1040
Dale, D. A., Helou, G., Magdis, G. E., et al. 2014, ApJ, 784, 83
Draine, B. T., & Li, A. 2007, ApJ, 657, 810
Elbaz, D., Daddi, E., Le Borgne, D., et al. 2007, A&A, 468, 33
Elbaz, D., Jahnke, K., Pantin, E., Le Borgne, D., & Letawe, G. 2009, A&A, 507, 1359
Feain, I. J., Papadopoulos, P. P., Ekers, R. D., & Middelberg, E. 2007, ApJ, 662, 872
Fritz, J., Franceschini, A., & Hatziminaoglou, E. 2006, MNRAS, 366, 767
Gaibler, V., Khochfar, S., Krause, M., & Silk, J. 2012, MNRAS, 425, 438
Heesen, V., Brinks, E., Leroy, A. K., et al. 2014, AJ, 147, 103

Heesen, V., Klocke, T. L., Brüggen, M., et al. 2023, A&A, 669, A8
Hirotani, K. 2005, ApJ, 619, 73
Imanishi, M., Ichikawa, K., Takeuchi, T., et al. 2011, PASJ, 63, 447
Kelly, B. C. 2007, ApJ, 665, 1489
Kovalev, Y. Y., Lobanov, A. P., Pushkarev, A. B., & Zensus, J. A. 2008, A&A, 483, 759
Krumholz, M. R., & Federrath, C. 2019, FrASS, 6, 7
Lammers, C., Iyer, K. G., Ibarra-Medel, H., et al. 2023, ApJ, 953, 26
Latif, M. A., Schleicher, D. R. G., Schmidt, W., & Niemeyer, J. 2013, MNRAS, 432, 668
Livio, M., Ogilvie, G. I., & Pringle, J. E. 1999, ApJ, 512, 100
Lobanov, A. P. 1998, A&A, 330, 79
McKee, C. F., & Ostriker, E. C. 2007, ARA&A, 45, 565
Mestel, L. 1965a, QJRAS, 6, 161
Mestel, L. 1965b, QJRAS, 6, 265
Niklas, S., & Beck, R. 1997, A&A, 320, 54
Noll, S., Burgarella, D., Giovannoli, E., et al. 2009, A&A, 507, 1793
O'Sullivan, S. P., & Gabuzda, D. C. 2009, MNRAS, 400, 26
Pushkarev, A. B., Hovatta, T., Kovalev, Y. Y., et al. 2012, A&A, 545, A113

Rodrìguez Zaurìn, J., Holt, J., Tadhunter, C. N., & González Delgado, R. M. 2007, MNRAS, 375, 1133
Schleicher, D. R. G., Banerjee, R., Sur, S., et al. 2010, A&A, 522, A115
Schleicher, D. R. G., & Beck, R. 2013, A&A, 556, A142
Schober, J., Schleicher, D., Federrath, C., et al. 2012, ApJ, 754, 99
Schutte, Z., & Reines, A. E. 2022, Natur, 601, 329
Skrutskie, M. F., Cutri, R. M., Stiening, R., et al. 2006, AJ, 131, 1163
Sokolovsky, K. V., Kovalev, Y. Y., Pushkarev, A. B., & Lobanov, A. P. 2011, A&A, 532, A38
Steinwandel, U. P., Dolag, K., Lesch, H., et al. 2020, MNRAS, 494, 4393
Tabatabaei, F. S., Minguez, P., Prieto, M. A., & Fernández-Ontiveros, J. A. 2018, NatAs, 2, 83
Tabatabaei, F. S., Schinnerer, E., Krause, M., et al. 2017, ApJ, 836, 185
Venturi, G., Treister, E., Finlez, C., et al. 2023, A&A, 678, A127
Wright, E. L., Eisenhardt, P. R. M., Mainzer, A. K., et al. 2010, AJ, 140, 1868
Zamaninasab, M., Clausen-Brown, E., Savolainen, T., & Tchekhovskoy, A. 2014, Natur, 510, 126
Zinn, P. C., Middelberg, E., Norris, R. P., & Dettmar, R. J. 2013, ApJ, 774, 66